

Light-Induced Quantum Anomalous Hall Effect on the 2D Surfaces of 3D Topological Insulators

Haowei Xu, Jian Zhou, and Ju Li*

Quantum anomalous Hall (QAH) effect generates quantized electric charge Hall conductance without external magnetic field. It requires both nontrivial band topology and time-reversal symmetry (TRS) breaking. In most cases, one can break the TRS of time-reversal invariant topological materials to yield QAH effect, which is essentially a topological phase transition. However, conventional topological phase transition induced by external field/stimulus usually needs a route along which the bandgap closes and reopens. Hence, the transition occurs only when the magnitude of field/stimulus is larger than a critical value. In this work the authors propose that using gapless systems, the transition can happen at an arbitrarily weak (but finite) external field strength. For such an unconventional topological phase transition, the bandgap closing is guaranteed by bulk-edge correspondence and symmetries, while the bandgap reopening is induced by external fields. This concept is demonstrated on the 2D surface states of 3D topological insulators like Bi_2Se_3 , which become 2D QAH insulators once a circularly polarized light is turned on, according to the Floquet time crystal theory. The sign of quantized Chern number can be controlled via the chirality of the light. This provides a convenient and dynamic approach to trigger topological phase transitions and create QAH insulators.

advantageous as light can be noncontact, nondestructive, and ultrafast. There are already several theoretical proposals and experimental observations that light (or focused laser pulses) can trigger structural phase transitions in both 3D bulk materials and low-dimensional nanostructures.^[1–3] In addition, light can also change the electronic structure and induce electronic phase transitions. In insulators or semiconductors, above-bandgap light can excite electron-hole pairs, and the system would acquire metallic properties in e.g., carrier transports. In a sense, this can be regarded as an insulator-to-metal transition. Indeed, the reverse process, metal-to-insulator phase transition under light, which is more counter-intuitive, has also been proposed.^[4]

In recent years, band topological orders (characterized by, e.g., Z_2 number) has become an important paradigm for material classifications. To date, hundreds of materials have been predicted to possess nontrivial electronic band topologies,^[5–7] and

some of them have already been fabricated and demonstrated in experiments. However, the quantum anomalous Hall (QAH) effect^[8,9] characterized by the Chern number $C \in \mathbb{Z}$, is still challenging for experimental observations. The QAH effect features an integer quantum Hall conductance $\sigma_{xy} = C \frac{e^2}{h}$ without external magnetic field, where e is the electron charge and h is the Planck constant. Notably, QAH insulators are rare in nature, due to two stringent, necessary, but not sufficient conditions, namely 1) inverted band structures near the Fermi level and 2) broken time-reversal symmetry (TRS).^[9] The first practical model for QAH insulators was proposed by Haldane.^[8] Then it was demonstrated that introducing magnetic dopant atoms into topological insulators (TIs) could break the TRS and lead to the QAH effect.^[10] In 2009, Chang et al. performed the first successful experiment and observed the QAH effect in Cr- or V-doped $(\text{Bi}, \text{Sb})_2\text{Te}_3$ thin films at very low temperature (≈ 80 mK).^[11] However, such extrinsic doping requires careful control over the impurity magnetic sites and interactions. Recently, it was found that intrinsic QAH effect can be observed in MnBi_2Te_4 thin films at an elevated temperature of 4 K.^[12–14] Despite these advances, more experimentally accessible materials and novel mechanisms to realize and observe QAH effect at high temperatures still need to be explored. In this work, we demonstrate that under circularly polarized light (CPL), quantum phase transition and 2D QAH effect

1. Introduction

Light has become a powerful tool for tuning material behaviors without direct contact. A promising application actively explored in recent years is light-driven phase transitions. Compared with conventional mechanical, thermal, electrical, or electrochemical approaches, using light as an external driving force is

H. Xu, Dr. J. Zhou, Prof. J. Li
Department of Nuclear Science and Engineering
Massachusetts Institute of Technology
Cambridge, MA 02139, USA
E-mail: liju@mit.edu

Prof. J. Li
Department of Materials Science and Engineering
Massachusetts Institute of Technology
Cambridge, MA 02139, USA

 The ORCID identification number(s) for the author(s) of this article can be found under <https://doi.org/10.1002/advs.202101508>

© 2021 The Authors. Advanced Science published by Wiley-VCH GmbH. This is an open access article under the terms of the Creative Commons Attribution License, which permits use, distribution and reproduction in any medium, provided the original work is properly cited.

DOI: 10.1002/advs.202101508

can be induced and controlled on the gapless surfaces of 3D TIs such as Bi_2Se_3 . We theoretically and computationally analyzed how the surface states evolve with light illumination and demonstrate how the anomalous Hall conductivity arises on the surfaces of TIs. We clarify that the Hall conductance under CPL only exists on the top and bottom layers of the Bi_2Se_3 slab, while the middle layers remain silent. Our work could provide more detailed evidence for careful experimental verifications and potential applications. In addition, we propose an unconventional pathway for topological phase transitions. We point out that in principle, an arbitrarily weak external field would be able to induce topological phase transitions in gapless systems, in contrast to the conventional topological phase transitions, where a finite and usually large external field is required. This unconventional topological phase transition is applicable in many gapless systems beyond the surface states of TIs.

2. Results

Considering the interaction between electrons and monochromatic light with frequency Ω , the electronic system has a time-periodic Hamiltonian $H(t) = H(t + T)$, where $T \equiv \frac{2\pi}{\Omega}$ is the period. The temporal periodicity is reminiscent of the spatial periodicity in crystals (translational symmetry), and can be systematically treated with the Floquet time-crystal theory^[15–18] analogous to Bloch's theorem. Intuitively, there can be virtual interactions between the system at time t and its temporal images at $t + mT$ ($m \in \mathbb{Z}$), similar to the interaction between an atom and its spatial image in neighboring unit cells. Such interaction provides a dynamical tool for tuning the properties of the system. When 1) the periodic perturbation is weak, and 2) its frequency Ω is much higher than the observational frequency (energy) scale so that no resonant transitions can happen, one can apply the high-frequency (van Vleck's) expansion, and obtain an effective time-independent Floquet Hamiltonian,

$$H^F \approx \tilde{H}^0 + \sum_{m \neq 0} \frac{[\tilde{H}^{-m}, \tilde{H}^m]}{2m\Omega} \quad (1)$$

where $\tilde{H}^m = \frac{1}{T} \int_0^T dt H(t) e^{im\Omega t}$ is the Fourier transform of $H(t)$. Here we only keep the lowest-order terms in the van Vleck's expansion. Utilizing the Floquet theory, it has been demonstrated that the electronic structures of the materials can be controlled with light,^[19,20] and particularly, topologically trivial materials could become topologically nontrivial under light illumination without structural (ionic) changes.^[21–24] For example, the anomalous Hall effect under CPL in graphene has been proposed^[21] and observed recently.^[25] It has also been proposed that light could induce effective spin-orbit coupling and trigger the quantum spin Hall to QAH transition in checkerboard antiferromagnetic superconductor FeSe monolayer.^[26] However, the transition requires ultra-strong light with AC electric field strength on the order of 1 V \AA^{-1} . Besides, free-standing FeSe monolayers are challenging to fabricate. Hence, it is desirable to explore the light-induced QAH effect 1) under lower light intensity and 2) in materials with better experimental feasibility. In this work, we propose that under CPL the 2D surface states of 3D Z_2 -TIs could show QAH effect. A unique advantage of starting from the 2D surface states of

TIs is that the intensity of the CPL required to trigger the quantum phase transition can be arbitrarily weak. This is because the 2D TI surface states are gapless by themselves and could easily transit to QAH insulators once their bandgaps are opened. This property may make experimental observations significantly easier. From a practical point of view, this could also reduce light absorption and the possible heating effects, especially when the light frequency is below the bulk bandgap and the electron-hole pair generation can be significantly reduced. Besides, the surface states are particularly sensitive to light at low frequencies (e.g., infrared or terahertz), and may find applications in light detection.

It is well known that topological electronic phase transitions can be triggered by external stimuli (denoted as F here), such as strain, electric field, light, etc. Except for some rare cases,^[27] a common and prominent feature of conventional topological phase transitions is that the bandgap of the material needs to close at a critical strength of the external field ($F = F_{\text{cri}}$) and then reopen as the field strength further increases ($F > F_{\text{cri}}$). On two sides of the critical strength ($F < F_{\text{cri}}$ and $F > F_{\text{cri}}$), the system usually has different topological properties, and the topological phase transition occurs at $F = F_{\text{cri}}$ (Figure 1a). This picture holds in the case of the transition from time-reversal symmetric TIs to QAH insulators as well. The TRS breaking field (induced by magnetic doping, etc.) needs to reach a critical value F_{cri} to trigger QAH phase. When the TRS breaking field is weak ($F < F_{\text{cri}}$), the Hall conductance remains zero in the system, even if the TRS is broken.^[28] This is verified in the case of both magnetic doping^[10] and CPL irradiation,^[26] where a finite critical external field strength is required to close and reopen the bandgap.

Notably, the magnitude of the critical field strength F_{cri} is usually not small. For example, it is on the order of a few percent elastic strain,^[29] a field strength of 1 V \AA^{-1} in the case of static electric field,^[30] and an intensity of $10^{12} \text{ W cm}^{-2}$ in the case of light-induced phase transitions.^[26] Such large critical field strengths hinder the observation and applications of topological phase transitions, and may also induce unwanted side effects. As discussed previously, when the field strength goes from $F = 0$ to $F = F_{\text{cri}}$, the bandgap reduces from the intrinsic value down to zero. Hence, a natural speculation is that, if the system is initially gapless, then the topological phase transition can happen at zero field strength ($F_{\text{cri}} = 0$), as the bandgap closing process is not required any more. In this case, once the external field is turned on (arbitrarily small strength), the system would immediately open its bandgap and transit to a different topological phase (Figure 1b). This can be understood with a thermodynamic phase transition picture. For the conventional topological phase transitions shown in Figure 1a, the initial system is located at a local minimum on the transition path, thus a finite F_{cri} is required to bring the system onto the (electronic) transition saddle point. On the other hand, if the topological phase transition starts from a gapless phase (Figure 1b), then the system is initially located on the transition saddle point, thus F_{cri} can be arbitrarily small.

Fortunately, some systems are guaranteed to be gapless. For example, the 2D surface states of a 3D Z_2 -TI are protected to be gapless when interfaced with topologically trivial systems (such as vacuum). This is because when continuously connecting two systems with different band topologies, the bandgap must close in between. Such gapless surface states are robust against

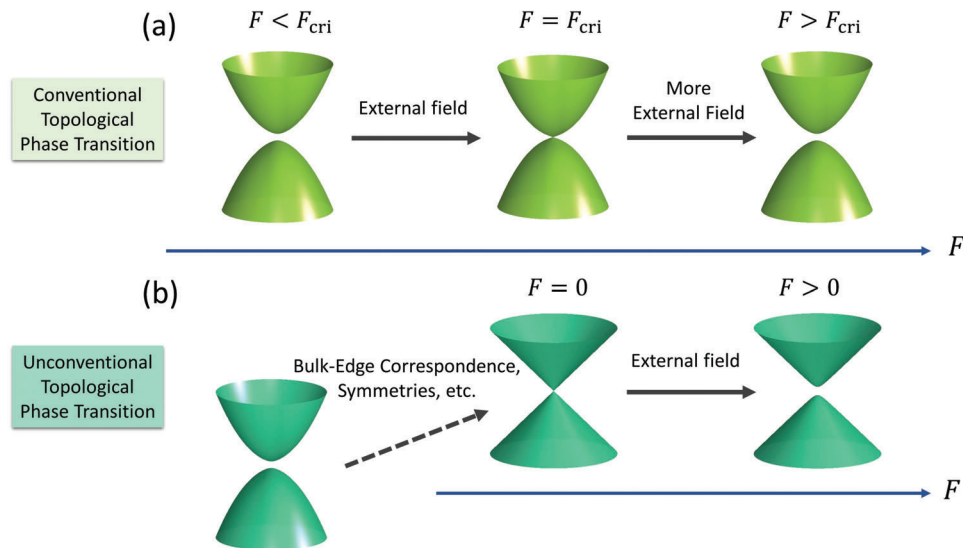


Figure 1. Two types of topological phase transitions. a) Conventional topological phase transition. The bulk bandgap closing and reopening processes are both triggered by external field F . And the topological phase transition occurs at a critical field strength F_{cri} , where the bandgap just closes. b) Unconventional topological phase transition. The bandgap closing is guaranteed by bulk-edge correspondence, symmetries, etc., whereas the bandgap reopening is induced by external field. Once the bandgap is opened, the system can change into a different topological state.

perturbations, disorders, and impurities that preserve TRS.^[31–33] However, when TRS is broken, the surface bandgaps could open and the QAH effect may arise. Therefore, one could start from these gapless surface states and trigger the QAH effect with CPL, which breaks TRS. Note that this topologically protected gapless state is different from graphene, since the latter one is not immune to external doping and requires high-quality fabrication process. Here we first study this effect with a minimal model Hamiltonian^[34] that can describe the surface states of TIs, $H_{\text{SS}}(\mathbf{k}) = \hbar v_{\text{F}}(k_x \sigma_y - k_y \sigma_x)$, which is essentially a 2D Dirac Fermion. Here v_{F} is the velocity of the Dirac Fermion, and σ_i ($i = x, y, z$) are the Pauli matrices. One can derive the effective Floquet Hamiltonian (see Supporting Information) under CPL irradiation as

$$H_{\text{SS}}^{\text{F}}(\mathbf{k}) = \hbar v_{\text{F}}(k_x \sigma_y - k_y \sigma_x) \pm \frac{e^2 v_{\text{F}}^2 \mathbf{A}^2}{\hbar \Omega} \sigma_z \quad (2)$$

where + and – correspond to right- and left-handed CPL, respectively. \mathbf{A} and Ω are the vector potential and the angular frequency of the CPL, respectively. The last term is induced by the CPL, and it represents an exchange field that breaks the TRS and opens a bandgap of $\frac{e^2 v_{\text{F}}^2 \mathbf{A}^2}{\hbar \Omega}$. It is well-known that Equation (2) describes QAH insulators^[8,35] with a Chern number of $C = \pm 1$. Note that here \mathbf{A} can be arbitrarily small. Besides, these results remain the same when the higher order terms are incorporated in the $k \cdot p$ model to reflect the warping from real lattice symmetries.^[36]

To illustrate the above toy model in a real material, we take bulk Bi_2Se_3 as an example, which is a well-studied Z_2 -TI.^[34,37] First-principles density functional theory calculation is performed to reproduce its electronic band structure more accurately than the toy model Hamiltonian above. The atomic structure of Bi_2Se_3 (Figure 2a) has a space group of $R\bar{3}m$ and has a layered structure along the z direction. Each layer is constituted by five atom layers

(Se-Bi-Se-Bi-Se), and is dubbed a quintuple layer (QL). The bulk of Bi_2Se_3 has a bandgap of ≈ 0.3 eV,^[34,37] while the surface states of Bi_2Se_3 are gapless. In Figure 2b we plot the electronic dispersion of its [111] surface, where a gapless Dirac dispersion at the $\bar{\Gamma}$ point can be seen. We now add a CPL propagating along the z direction, with time-dependent vector potential $\mathbf{A}(t) = A(\cos \Omega t, \eta \sin \Omega t, 0)$, where $\eta = +1$ and -1 correspond to left- and right-handed CPL, respectively. We take $\hbar \Omega = 5$ eV for the following calculations, which is much higher than the frequency (energy) range of interest in this work. Here we would like to remark that a smaller frequency (especially below the bandgap ≈ 0.3 eV) may be more favorable in experiments. We adopt $\Omega = 5$ eV mainly from a computational point of view, as the theoretical error from the van Vleck's expansion would be smaller at this high frequency. In Figure 2c we plot the surface spectrum function under left-handed CPL with intensity of $\frac{eA}{\hbar} = 0.1 \text{ \AA}^{-1}$ (corresponding to an electric field strength of $E = 5 \text{ V nm}^{-1}$), which is calculated based on the Floquet formalism (see Supporting Information). A bandgap of $E_{\text{g}} \approx 20$ meV can be clearly observed. We then adjust the light intensity and explore its relationship with the bandgap. When the light is not too strong, the bandgap scales as $E_{\text{g}} \propto A^2 \propto I$, where I is the light intensity (Figure 2d). This relationship is intuitive as I characterizes the strength of TRS breaking. Also, the bandgap opening is a second-order nonlinear effect induced by the photo-dressing of the electronic states, hence E_{g} should be linearly proportional to I , which is also proportional to the number of photons irradiated. However, for a strong light with $\frac{eA}{\hbar} \gtrsim 0.2 \text{ \AA}^{-1}$, the fundamental bandgap tends to decrease as the light intensity increases. When the light is strong enough, the system becomes metallic. This is due to the interplay between different orbitals in Bi_2Se_3 , and is absent when one uses a low-energy effective Hamiltonian as described above, which involves only a subset of the atomic orbitals near the Fermi level. On the other hand, when a linearly polarized light is applied,

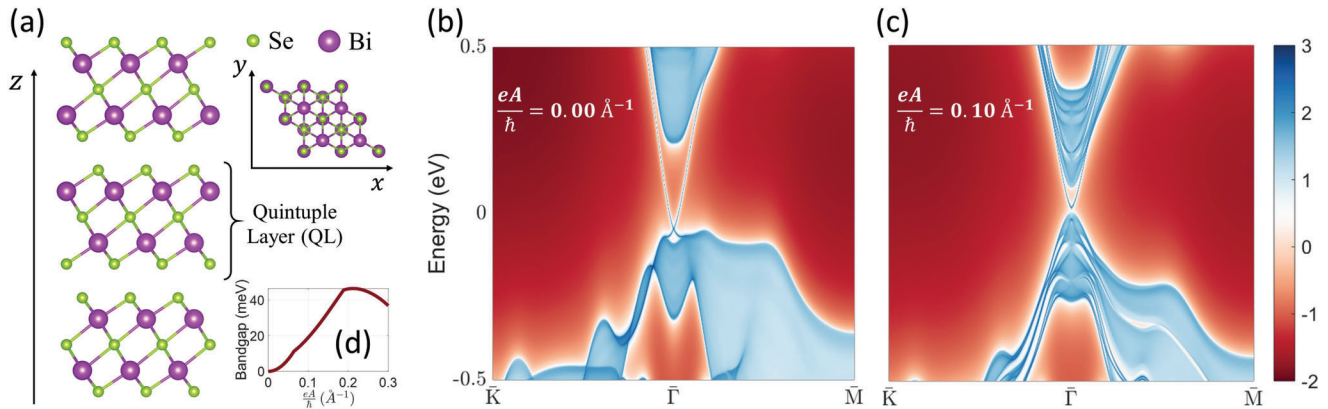


Figure 2. a) Atomic structure of Bi_2Se_3 . The surface state spectrum of Bi_2Se_3 under b) no light and c) CPL with field strength $\frac{eA}{\hbar} = 0.1 \text{ \AA}^{-1}$, respectively. A bandgap of 20 meV can be seen in (c). Note that the colormap in (b, c) is in logarithmic scale. d) Bandgap of the surface states of Bi_2Se_3 as a function of the CPL strength. The bandgaps are calculated with a slab model with 24 QLs.

which does not break TRS, the surface states remain gapless (Figure S1, Supporting Information).

Usually, bandgap closing and opening correspond to topological phase transitions. To quantify the topological nature of the Bi_2Se_3 surface state under CPL, we calculate its Hall conductance, according to the Kubo formula,

$$\sigma_{ab} = \frac{e^2}{\hbar} \sum_{n \neq m} \int_{\text{BZ}} \frac{dk}{(2\pi)^2} (f_{nk} - f_{mk}) \frac{\text{Im} \{ \langle mk | v_a | nk \rangle \langle nk | v_b | mk \rangle \}}{(\omega_{mk} - \omega_{nk})^2} \quad (3)$$

Here $|nk\rangle$, ω_{nk} and f_{nk} are the eigenstates, eigenvalues (band frequency), and occupancy of the n -th band of the Floquet Hamiltonian $H^F(\mathbf{k})$, respectively. $v_a = \frac{1}{\hbar} \frac{\partial H^F}{\partial k_a}$ with $a = x, y$ is the velocity operator. A slab model is used to calculate the Hall conductance. Specifically, we first build an intrinsic Hamiltonian H for Bi_2Se_3 from ab initio calculations, and then evaluate the effective Hamiltonian H^F under light using the van Vleck's expansion. In the current case, we need to resolve the contributions to the conductivity from each QL in the system. We define a spatial projection operator $P_l = \sum_{i \in l} |\psi_i\rangle \langle \psi_i|$. Here $|\psi_i\rangle$ are atomic orbitals, and the summation runs over all orbitals centered on the l -th QL. Then we replace the current operator v_a with $P_l v_a$, which corresponds to the current localized on the l -th QL. In this way, a layer-resolved conductance σ_{ab}^l can be obtained. Note that by summing over l , the total conductance of the whole slab can be recovered. Here we would like to note that in the periodically driven system, the electrons are usually out-of-equilibrium. As a result, Equation (3) should be considered as an approximation to the dynamic Hall conductivity, with a correction up to the order of (A^2) . Such an approximation requires^[38] that 1) the frequency of light is off-resonance so that the direct interband transitions is marginal; 2) the intensity of light A^2 is small. Both of them are satisfied in the present work. In general cases where resonant interband transitions can happen, or A^2 is large, the occupation of the Floquet bands can significantly deviate from the Fermi-Dirac distribution and one should apply the Floquet theory in a more rigorous fashion.^[39–41] Generally speaking, the Hall conductivity is ex-

pected to be nonzero, but it may deviate from the quantized value, depending on the actual experimental conditions. We would like to note again that the choice of light frequency $\Omega = 5 \text{ eV}$ in this work is mainly from a theoretical and computational standpoint, but the essence of our results holds true at lower frequencies. At low frequencies, a bandgap of 20 meV can be obtained under a small electric field strength (see Supporting Information). Actually, in Ref. ^[42] a CPL with $\Omega = 0.12 \text{ eV}$ and $E = 2.5 \times 10^7 \text{ Vm}^{-1}$ was used, and a bandgap of $E_g \approx 50 \text{ meV}$ was observed on the surfaces of Bi_2Se_3 . Under these conditions, our ab initio calculation predicts a bandgap of $E_g \approx 35 \text{ meV}$ according to the van Vleck's expansion. This demonstrates that the van Vleck's expansion can give a qualitatively correct result even with low light frequency.

We first use a slab model with 24 QLs, which is thick enough to rule out the interaction between the top and bottom surfaces. Under left-handed CPL with $\frac{eA}{\hbar} = 0.1 \text{ \AA}^{-1}$, the calculated layer-resolved Hall conductance $\frac{1}{2}(\sigma_{xy}^l - \sigma_{yx}^l)$ is shown in Figure 3. Here the green dots represent the layer-resolved conductance, whereas the red dots show the total conductance measured from the first QL to the l -th QL, that is, $\sum_{i=1}^l \frac{1}{2}(\sigma_{xy}^i - \sigma_{yx}^i)$. From Figure 3a, one can see that the whole slab system has a quantized Hall conductance of $-\frac{e^2}{h}$. Remarkably, only the top and bottom surfaces (roughly 6 QLs) contribute to σ_{xy} ; each gives $-0.5 \frac{e^2}{h}$. Under right-handed CPL, the Hall conductivity flips its sign (Figure 3b). Thus, the system has Chern number $C = +1$ and -1 under right- and left-handed CPL, respectively. This demonstrates that the whole slab becomes a QAH system when the bandgap is opened under CPL irradiation. Hence, the light serves as an effective SOC interaction. The strength and sign of this effective SOC can be fine-tuned via light intensity and handedness. This is different from the usual atomic SOC interaction, which is determined mainly by the atomic number and is also positive, leaving little room for tunability. On the other hand, QLs in the middle of the slab remain silent and have almost zero Hall conductance. We also calculated the spin Hall conductance, and find that each middle QL gives a spin Hall conductance of $0.36 \frac{\hbar}{2e} \frac{e^2}{h}$ (see Supporting Information), which is close to the layer-resolved spin Hall conductance in a bulk Bi_2Se_3 . This again suggests that although the CPL breaks the TRS in the middle QLs, it is not strong enough to

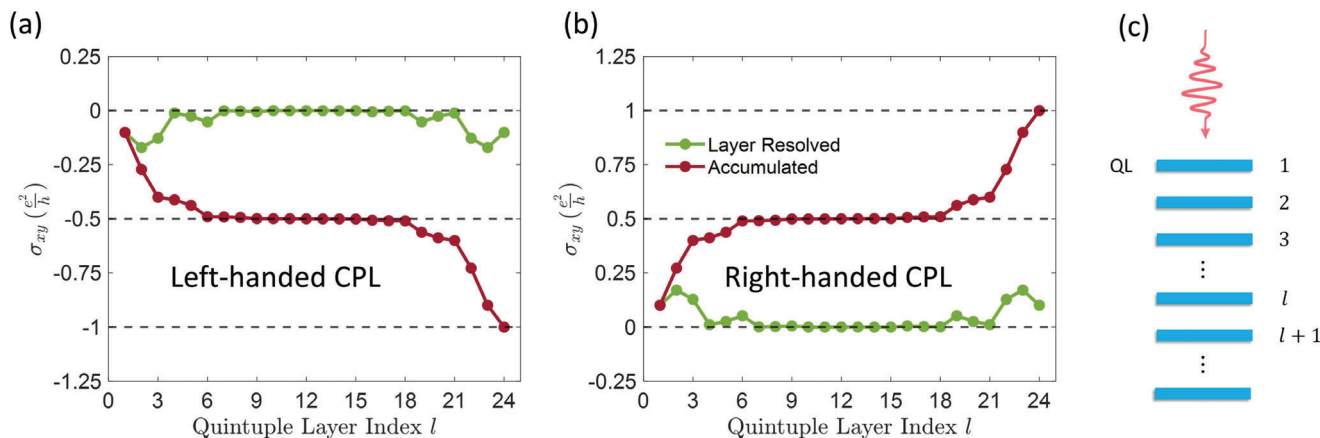


Figure 3. Layer-resolved Hall conductance of a Bi₂Se₃ slab with 24 QLs under a) left-handed and b) right-handed CPL with $\frac{eA}{h} = 0.1 \text{ \AA}^{-1}$. The top and bottom surface each contributes $0.5 \frac{e^2}{h}$, and the whole slab is a QAH insulator. The green dots represent layer-resolved Hall conductance of each layer indexed by l , while the red dots are summation of Hall conductance from the 1st (top) to the l th layers. c) A schematic illustration of the Bi₂Se₃ slab under light.

trigger the phase transition to the QAH insulator with the conventional pathway depicted in Figure 1a. However, the transition can be triggered on the surfaces with the unconventional pathway in Figure 1b, because one does not need a finite critical field to close the bandgap on the surfaces.

To better understand the thickness effect and demonstrate the benefit of using the gapless surface states, we consider a thin slab of Bi₂Se₃ as a comparison. In the thin-slab scenario, the quantum tunneling between the top and bottom surface states leads to a mass term and opens a bandgap. Specifically, the bandgap of a slab with 6 QLs is around 4 meV. When we turn on the CPL, the bandgap gradually decreases (Figure 4), but the Hall conductance remains zero until the bandgap closes at a critical field strength $\frac{eA_{crit}}{h} \approx 0.05 \text{ \AA}^{-1}$. With $\frac{eA}{h} > 0.05 \text{ \AA}^{-1}$, the system becomes a QAH

insulator with Hall conductance of $-\frac{e^2}{h}$. This is a vivid illustration of the conventional topological phase transitions depicted in Figure 1a, which cannot happen below a critical field strength. When we use a thicker slab, then the bandgap $\rightarrow 0$, the critical field strength $\rightarrow 0$, and we recover our main proposition. On the other hand, if we use a thinner slab, then the critical light intensity required to trigger the phase transition would be even higher. For example, if we use 3 QLs, then the intrinsic bandgap is around 50 meV, and the transition to a QAH state cannot happen even when $\frac{eA}{h}$ is 0.15 \AA^{-1} .

3. Discussion and Conclusion

Before concluding, we would like to make several remarks. First, the influence of CPL can also be interpreted as being caused by the inverse Faraday effect.^[43] It is well-known that the CPL can induce an effective magnetic field (or equivalently, an effective magnetization), which would naturally induce a Hall conductance. This is also consistent with the analysis above that CPL induces an exchange interaction (Equation (2)). On the other hand, in Ref. ^[43] it was demonstrated that not only a CPL but also a linearly polarized light could lead to a nonzero static magnetization. This occurs when the frequency of the linearly polarized light is above the electronic bandgap. In this case, the electron interband transitions would cause energy dissipations, which breaks the TRS according to the second law of thermodynamics.^[43] From this point of view, a linearly polarized light might also lead to the QAH effect on the surfaces of topological materials, provided that the dissipations are taken into consideration.^[43,44] Such possibility will be studied in a future work.

Second, the unconventional topological phase transition may be used for light detection, especially in the low-frequency range (e.g., terahertz). As discussed above, the bandgap opened by the CPL is $E_g \propto \frac{A^2}{\Omega} \propto \frac{I}{\Omega^2}$, where I and Ω are intensity and frequency of the light, respectively. The $E_g \propto \Omega^{-3}$ scaling law indicates that the surface states are particularly sensitive to light with relatively low frequencies. This should be compared with conventional

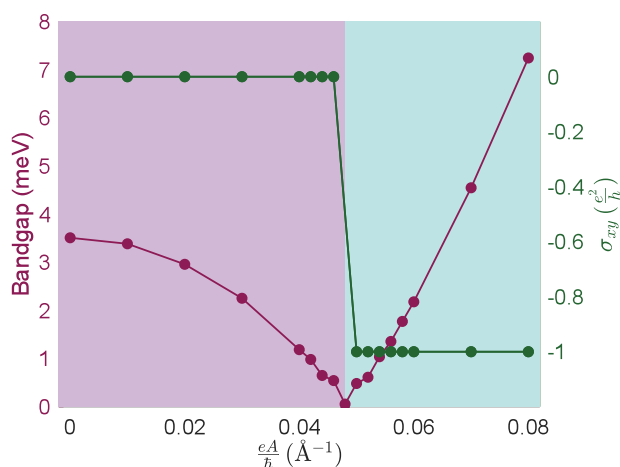


Figure 4. The bandgap (left y-axis) and Hall conductance (right y-axis) of a Bi₂Se₃ slab with 6 QLs as a function of the field strength of the left-handed CPL. The system has finite bandgap and zero Hall conductance before light illumination. A transition to QAH insulator happens at $\frac{eA}{h} \approx 0.05 \text{ \AA}^{-1}$, where the bandgap closes and reopens.

approaches for light detection, whose sensitivity usually decreases as the light frequency decreases. Low frequencies below the bulk bandgap have another advantage that the absorption in the bulk can be avoided. Of course, at very low frequencies, one should use the Floquet theory in a more formal way than the high-frequency van Vleck's expansion used in the current work, but the stronger sensitivity at low frequencies should be qualitatively true. In addition, at very low frequencies, other unwanted processes, such as the coupling with phonons, may come into play. A thorough consideration of these effects will be the focus of the future works. Besides, the sharp jump of the Hall conductance σ_{xy} from 0 to $\frac{e^2}{h}$ can be detected by optical approaches such as magneto-optical Kerr or Faraday rotation, which can make a possible all-optical light detection device.

Finally, this unconventional topological phase transition may also apply to other gapless systems, such as the surface states of topological crystalline insulators^[45,46] or Dirac semimetals.^[47] In these systems, the zero bandgaps are protected by crystal spatial symmetries, hence the topological properties may strongly couple with phonons, which can break certain crystal symmetries. Thus, these systems could be ideal platforms for studying phonon-dressed electronic states dynamically.

In conclusion, we demonstrate that the 2D surface states of 3D TIs can transit to QAH insulators under CPL irradiation. A prominent feature is that the critical light strength required to trigger the surface electronic-state phase transition can be arbitrarily small since the surface bandgap is already closed according to the bulk-edge correspondence. Such an unconventional topological phase transition can make easier experimental observations of QAH effects under high temperature, and may find practical applications such as light detection. Intuitively, one may think of the CPL as generating effective magnetism on the gapless surface,^[43,44] thus giving rise to the QAH effect.

Supporting Information

Supporting Information is available from the Wiley Online Library or from the author.

Acknowledgements

This work was supported by the Office of Naval Research Multidisciplinary University Research Initiative Award No. ONR N00014-17-1-2661.

Conflict of Interest

The authors declare no conflict of interest.

Data Availability Statement

The data that support the findings of this study are available from the corresponding author upon reasonable request.

Keywords

DFT calculations, Floquet theory, quantum anomalous Hall effect, topological insulators

Received: April 12, 2021

Revised: May 8, 2021

Published online: July 2, 2021

- [1] J. Zhou, H. Xu, Y. Li, R. Jaramillo, J. Li, *Nano Lett.* **2018**, *18*, 7794.
- [2] J. Shi, Y.-Q. Bie, W. Chen, S. Fang, J. Han, Z. Cao, T. Taniguchi, K. Watanabe, V. Bulović, E. Kaxiras, P. Jarillo-Herrero, K. A. Nelson, **2019**, *arXiv:1910.13609*.
- [3] J. Zhang, J. Han, G. Peng, X. Yang, X. Yuan, Y. Li, J. Chen, W. Xu, K. Liu, Z. Zhu, W. Cao, Z. Han, J. Dai, M. Zhu, S. Qin, K. S. Novoselov, *Light: Sci. Appl.* **2020**, *9*, 2047.
- [4] I. Esin, M. S. Rudner, N. H. Lindner, *Sci. Adv.* **2020**, *6*, eaay4922.
- [5] T. Zhang, Y. Jiang, Z. Song, H. Huang, Y. He, Z. Fang, H. Weng, C. Fang, *Nature* **2019**, *566*, 475.
- [6] M. G. Vergniory, L. Elcoro, C. Felser, N. Regnault, B. A. Bernevig, Z. Wang, *Nature* **2019**, *566*, 480.
- [7] F. Tang, H. C. Po, A. Vishwanath, X. Wan, *Nature* **2019**, *566*, 486.
- [8] F. D. M. Haldane, *Phys. Rev. Lett.* **1988**, *61*, 2015.
- [9] C.-X. Liu, S.-C. Zhang, X.-L. Qi, *Annu. Rev. Condens. Matter Phys.* **2016**, *7*, 301.
- [10] R. Yu, W. Zhang, H. J. Zhang, S. C. Zhang, X. Dai, Z. Fang, *Science* **2010**, *329*, 61.
- [11] C. Z. Chang, J. Zhang, X. Feng, J. Shen, Z. Zhang, M. Guo, K. Li, Y. Ou, P. Wei, L. L. Wang, Z. Q. Ji, Y. Feng, S. Ji, X. Chen, J. Jia, X. Dai, Z. Fang, S. C. Zhang, K. He, Y. Wang, L. Lu, X. C. Ma, Q. K. Xue, *Science* **2013**, *340*, 167.
- [12] M. M. Otrokov, I. I. Klimovskikh, H. Bentmann, D. Estyunin, A. Zeugner, Z. S. Aliev, S. Gaß, A. U. B. Wolter, A. V. Koroleva, A. M. Shikin, M. Blanco-Rey, M. Hoffmann, I. P. Rusinov, A. Y. Vyazovskaya, S. V. Ereemeev, Y. M. Koroteev, V. M. Kuznetsov, F. Freyse, J. Sánchez-Barriga, I. R. Amiraslanov, M. B. Babanly, N. T. Mamedov, N. A. Abdullayev, V. N. Zverev, A. Alfonso, V. Kataev, B. Büchner, E. F. Schwier, S. Kumar, A. Kimura, et al., *Nature* **2019**, *576*, 416.
- [13] J. Li, Y. Li, S. Du, Z. Wang, B. L. Gu, S. C. Zhang, K. He, W. Duan, Y. Xu, *Sci. Adv.* **2019**, *5*, eaaw5685.
- [14] D. Zhang, M. Shi, T. Zhu, D. Xing, H. Zhang, J. Wang, *Phys. Rev. Lett.* **2019**, *122*, 206401.
- [15] J. H. Shirley, *Phys. Rev.* **1965**, *138*, B979.
- [16] H. Sambe, *Phys. Rev. A* **1973**, *7*, 2203.
- [17] A. Eckardt, *Rev. Mod. Phys.* **2017**, *89*, 011004.
- [18] U. de Giovannini, H. Hübener, *arXiv* **2019**, *3*, 12001.
- [19] B. M. Fregoso, Y. H. Wang, N. Gedik, V. Galitski, *Phys. Rev. B: Condens. Matter Mater. Phys.* **2013**, *88*, 155129.
- [20] L. Bucciattini, S. Roy, S. Kitamura, T. Oka, *Phys. Rev. B* **2017**, *96*, 041126.
- [21] T. Oka, H. Aoki, *Phys. Rev. B: Condens. Matter Mater. Phys.* **2009**, *79*, 081406.
- [22] J. I. Inoue, A. Tanaka, *Phys. Rev. Lett.* **2010**, *105*, 017401.
- [23] N. H. Lindner, G. Refael, V. Galitski, *Nat. Phys.* **2011**, *7*, 490.
- [24] H. Liu, J. T. Sun, C. Cheng, F. Liu, S. Meng, *arXiv* **2017**, *120*, 237403.
- [25] J. W. McIver, B. Schulte, F. U. Stein, T. Matsuyama, G. Jotzu, G. Meier, A. Cavalleri, *Nat. Phys.* **2020**, *16*, 38.
- [26] Z. F. Wang, Z. Liu, J. Yang, F. Liu, *Phys. Rev. Lett.* **2018**, *120*, 156406.
- [27] M. Ezawa, Y. Tanaka, N. Nagaosa, *Sci. Rep.* **2013**, *3*, 2790.
- [28] Y. Yang, Z. Xu, L. Sheng, B. Wang, D. Y. Xing, D. N. Sheng, *Phys. Rev. Lett.* **2011**, *107*, 066602.
- [29] H. Aramberri, M. C. Muñoz, *Phys. Rev. B* **2017**, *95*, 205422.
- [30] X. Qian, J. Liu, L. Fu, J. Li, *Science* **2014**, *346*, 1344.
- [31] M. Z. Hasan, C. L. Kane, *Rev. Mod. Phys.* **2010**, *82*, 3045.
- [32] X. L. Qi, S. C. Zhang, *Rev. Mod. Phys.* **2011**, *83*, 1057.

- [33] A. Bansil, H. Lin, T. Das, *Rev. Mod. Phys.* **2016**, *88*, 021004.
- [34] H. Zhang, C. X. Liu, X. L. Qi, X. Dai, Z. Fang, S. C. Zhang, *Nat. Phys.* **2009**, *5*, 438.
- [35] X. L. Qi, T. L. Hughes, S. C. Zhang, *Phys. Rev. B: Condens. Matter Mater. Phys.* **2008**, *78*, 195424.
- [36] L. Fu, *Phys. Rev. Lett.* **2009**, *103*, 266801.
- [37] Y. Xia, D. Qian, D. Hsieh, L. Wray, A. Pal, H. Lin, A. Bansil, D. Grauer, Y. S. Hor, R. J. Cava, M. Z. Hasan, *Nat. Phys.* **2009**, *5*, 398.
- [38] T. Kitagawa, T. Oka, A. Brataas, L. Fu, E. Demler, *Phys. Rev. B: Condens. Matter Mater. Phys.* **2011**, *84*, 235108.
- [39] H. Deghani, T. Oka, A. Mitra, *Phys. Rev. B: Condens. Matter Mater. Phys.* **2014**, *90*, 195429.
- [40] K. I. Seetharam, C. E. Bardyn, N. H. Lindner, M. S. Rudner, G. Refael, *Phys. Rev. X* **2015**, *5*, 041050.
- [41] T. Iadecola, T. Neupert, C. Chamon, *Phys. Rev. B: Condens. Matter Mater. Phys.* **2015**, *91*, 235133.
- [42] Y. H. Wang, H. Steinberg, P. Jarillo-Herrero, N. Gedik, *Science* **2013**, *342*, 453.
- [43] H. Xu, J. Zhou, H. Wang, J. Li, *Phys. Rev. B* **2021**, *103*, 205417.
- [44] H. Xu, H. Wang, J. Zhou, J. Li, **2020**, *arXiv:2006.16945*.
- [45] L. Fu, *Phys. Rev. Lett.* **2011**, *106*, 106802.
- [46] T. H. Hsieh, H. Lin, J. Liu, W. Duan, A. Bansil, L. Fu, *Nat. Commun.* **2012**, *3*, 982.
- [47] N. P. Armitage, E. J. Mele, A. Vishwanath, *Rev. Mod. Phys.* **2018**, *90*, 015001.



Supporting Information

for *Adv. Sci.*, DOI: 10.1002/advs.202101508

Floquet quantum anomalous Hall effect on the surfaces of topological insulators

Haowei Xu, Jian Zhou, and Ju Li

Supplementary Information

of

Floquet quantum anomalous Hall effect on the surfaces of topological insulators

Haowei Xu¹, Jian Zhou¹, and Ju Li^{1,2}

¹Department of Nuclear Science and Engineering, Massachusetts Institute of Technology,
Cambridge, Massachusetts 02139, USA

²Department of Materials Science and Engineering, Massachusetts Institute of Technology,
Cambridge, Massachusetts 02139, USA

1 Methods

1.1 *Ab initio* calculations

The first-principles calculations in this work are based on density functional theory (DFT) [1, 2] implemented in Vienna ab initio simulation package (VASP) [3, 4]. The exchange-correlation interactions are treated by generalized gradient approximation (GGA) in the form of Perdew-Burke-Ernzerhof (PBE) [5]. Core electrons are treated with projected augmented wave (PAW) method [6], while the valence electrons are treated by a plane wave basis set with cutoff energy of 300 eV for Bi₂Se₃. The first Brillouin zone is sampled by a $13 \times 13 \times 5$ Γ -center k -mesh for the conventional standard unitcell of Bi₂Se₃.

1.2 Tight-binding Hamiltonian

The Bloch wavefunctions from DFT calculations described above are then used to build a tight-binding Hamiltonian with the Wannier90 package [7]. The atomic orbitals are defined with

$$|nR\rangle = \frac{1}{N} \sum_k e^{-ik \cdot R} \sum_{m=1}^J U_{mn}^k |mk\rangle \quad (\text{S1})$$

where $|mk\rangle$ is the Bloch wavefunctions from DFT, R are Bravais lattice vectors, J is the number of atomic orbitals in a unit cell. We use the p_x, p_y and p_z orbitals of Bi and Se to build the tight-binding Hamiltonian. U_{mn}^k is a unitary transformation. Note that when using Wannier90 we did not minimize the spread the wavefunctions (by setting num_iter = 0) in order to avoid incorrectly mixing spin up and down states of the spinor wavefunctions from VASP.

The time-independent tight-binding wavefunctions are

$$H_{mnR} = \langle m0|H|nR\rangle \quad (\text{S2})$$

1.3 Floquet theory

According to the Peierls substitution, under a periodic field $A(r, t)$, the time-dependent tight-binding Hamiltonian should become

$$\begin{aligned} \langle m0|\tilde{H}(t)|nR\rangle &= \langle m0|H|nR\rangle e^{-\frac{ie}{\hbar} \int_{\tau_n+R}^{\tau_m} A(r, t) \cdot dr} \\ &= \langle m0|H|nR\rangle e^{\frac{ie}{\hbar} A \cdot (R+\tau_n-\tau_m)} \end{aligned} \quad (\text{S3})$$

where τ_n is the center of the orbital $|n0\rangle$, $e = -|e|$ is the charge of the electron. Here we have assumed that A is spatially uniform.

Then as usual, the Bloch waves can be built from the atomic orbitals with

$$|nk\rangle = \frac{1}{\sqrt{N}} \sum_R e^{ik \cdot (R+\tau_n)} |nR\rangle \quad (\text{S4})$$

After some algebras, one can obtain the time-dependent Hamiltonian in the basis of Bloch waves as

$$\begin{aligned} \tilde{H}(k, t) &= \langle mk|\tilde{H}(t)|nk\rangle \\ &= \sum_R e^{(k+\frac{e}{\hbar}A) \cdot (R+\tau_n-\tau_m)} \langle m0|H|nR\rangle \\ &= H\left(k + \frac{e}{\hbar}A(t)\right) \end{aligned} \quad (\text{S5})$$

For a A periodic in time with periodicity T , the Fourier transform of $\tilde{H}(k, t)$ should be

$$\begin{aligned}\tilde{H}^m(k) &= \frac{1}{T} \int_0^T e^{-im\omega t} \tilde{H}(k, t) dt \\ &= \frac{1}{T} \int_0^T e^{-im\omega t} H\left(k + \frac{e}{\hbar} A(t)\right) dt\end{aligned}\tag{S6}$$

where $\Omega = 2\pi/T$ is the angular frequency. Then an effective Floquet Hamiltonian in the high frequency approximation is [8, 9, 10, 11]

$$H_{\text{eff}}^F = \tilde{H}^0 + \sum_{m \neq 0} \frac{[\tilde{H}^{-m}, \tilde{H}^m]}{2m\hbar\Omega}\tag{S7}$$

One straightforward method for obtaining $\tilde{H}^m(k)$ is to numerically compute the time integral in Eq. (S6). An advantage of this method is that all frequency components can be obtained in the same fashion, and the Floquet Hamiltonian H^F with arbitrary order can be obtained. Another method that is computationally more efficient is to expand Eq. (S6) as

$$\begin{aligned}\tilde{H}(k, t) &= H\left(k + \frac{e}{\hbar} A(t)\right) \\ &= H(k) + \left(\frac{e}{\hbar}\right) \frac{\partial H}{\partial k_i} A_i + \frac{1}{2} \left(\frac{e}{\hbar}\right)^2 \frac{\partial^2 H}{\partial k_i \partial k_j} A_i A_j + \dots\end{aligned}\tag{S8}$$

Assuming that A_i is monochromatic, to obtain a H_{eff}^F up to the order of A^2 , we only need to keep the first three terms in Eq. (S8), and $m = 1$ in Eq. (S7). Let

$$\begin{aligned}A_i &= A_i^0 \cos(\Omega t + \phi_i) \\ &= A_i^0 \frac{\eta_i e^{i\Omega t} + \eta_i^* e^{-i\Omega t}}{2}\end{aligned}\tag{S9}$$

where $\eta_i = e^{i\phi_i}$. One can obtain that

$$\begin{aligned}\tilde{H}^0(k) &= H(k) + \left(\frac{e}{\hbar}\right)^2 \sum_{ij} \frac{\partial^2 H}{\partial k_i \partial k_j} \frac{A_i^0 A_j^0}{4} (\eta_i \eta_j^* + \eta_i^* \eta_j) \\ [\tilde{H}^{-1}(k)]^\dagger = \tilde{H}^1(k) &= \left(\frac{e}{\hbar}\right) \sum_i \frac{\partial H}{\partial k_i} \frac{A_i^0}{2} \eta_i\end{aligned}\tag{S10}$$

Note that the Taylor expansion in Eq. (S8) is valid only when $\frac{e}{\hbar} A$ is small as compared with the size of the Brillouin zone, which is on the order of \AA^{-1} . With $\omega = 1$ eV and $E = 1$ V/nm, one has $\frac{e}{\hbar} A \approx 0.1 \text{\AA}^{-1}$. Hence the expansion is generally valid.

The interaction between electrons and light is mainly attributed to the $[H^{-1}, H^1]$, which describes the process that a photon is first virtually absorbed, and then virtually emitted by the electron. For a linearly polarized light (LPL), one can easily verify that $[H^{-1}, H^1]$ is zero. Therefore LPL cannot significantly change the electronic structure. Also, LPL preserves the time-reversal symmetry and

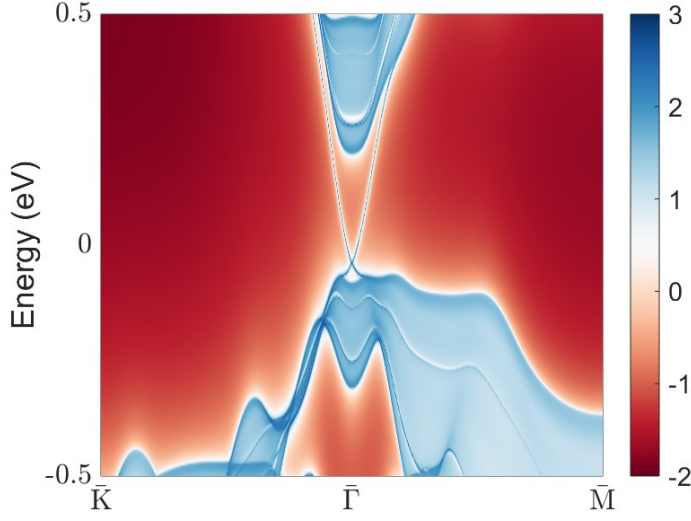


Figure S1: The surface spectrum function of Bi_2Se_3 under linearly polarized light. Note that linearly polarized light cannot open bandgaps on the surface states.

cannot open bandgaps on the surface states of topological materials. This is verified by our calculations (Figure S1).

As discussed in the main text, the model Hamiltonian for the surface states of topological insulators is

$$H_{\text{SS}}(k) = \hbar v_F (k_x \sigma_y - k_y \sigma_x) \quad (\text{S11})$$

Here one has $\frac{\partial H}{\partial k_x} = \hbar v_F \sigma_y$ and $\frac{\partial H}{\partial k_y} = -\hbar v_F \sigma_x$, while all other higher order derivatives of H with respect to k are zero. Thus one has

$$[\tilde{H}^{-1}(k)]^\dagger = \tilde{H}^1(k) = \frac{e v_F}{2} (A_x \eta_x \sigma_y - A_y \eta_y \sigma_x) \quad (\text{S12})$$

For a CPL, one should have $A_x = A_y = A$, $\eta_x = 1$, and $\eta_y = \pm i$. It is not hard to show that

$$[\tilde{H}^{-1}(k), \tilde{H}^1(k)] = \pm e^2 v_F^2 A^2 \sigma_z \quad (\text{S13})$$

Putting Eq. (S13) back to Eq. (S7), one can obtain Eq. (2) in the main text.

2 Responses under light with low frequency

In the main text we used $\Omega = 5$ eV for all the calculations with Bi_2Se_3 . Actually, one can (maybe improperly) apply the van Vleck's expansion to light with low frequency. Here we show the results

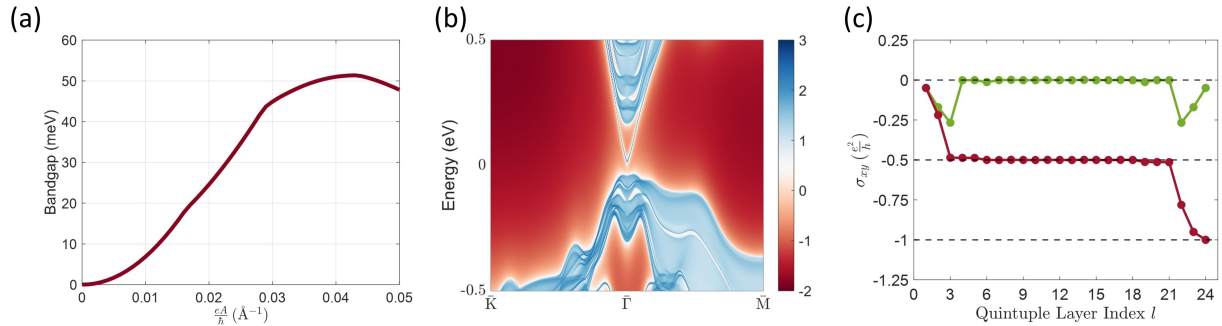


Figure S2: The surface states of Bi_2Se_3 under light with frequency $\Omega = 0.2$ eV. (a) Bandgap v.s. electric field strength at $\Omega = 0.2$ eV. (b) Surface states spectrum at $\Omega = 0.2$ eV and $\frac{eA}{\hbar} = 0.04$ \AA^{-1} . (c) Layer-resolved Hall conductance at $\Omega = 0.2$ eV and $\frac{eA}{\hbar} = 0.04$ \AA^{-1} .

with $\Omega = 0.2$ eV in Figure S2. One can see that the results are essentially the same as those with $\Omega = 5$ eV; that is, under circularly polarized light a bandgap is opened on the surfaces, and the surfaces acquire a quantized anomalous Hall conductance. Also, at $\Omega = 0.2$ eV, an electric field strength of $\frac{eA}{\hbar} = 0.015$ \AA^{-1} ($E = 0.03$ V/nm, $I = 12$ MW/cm²) would be able to generate a bandgap of 20 meV. On the other hand, at $\Omega = 5$ eV, it takes $E = 5$ V/nm, $I = 3.3 \times 10^6$ MW/cm² to generate the same bandgap.

When using the van Vleck's expansion at low frequencies, two sources of errors should be considered: 1) the interband transitions would lead to a non-thermal distribution of the electrons. In other words, one cannot simply use the Fermi-Dirac distribution. As light is turned on, the electrons are gradually pumped from the valence bands to the conduction bands. It takes time for the electron distribution to deviate significantly from the original Fermi-Dirac distribution. Specifically, if the pumping rate is R , then the distribution deviation is $\delta f \propto Rt$. Thus, one should expect that the Fermi-Dirac distribution is valid at the very initial stage ($t \ll 1/R$, which may be a few femtoseconds). 2) there is a correction to the effective Hamiltonian H_{eff} whose relative magnitude is on the order of $\frac{A}{\Omega}$. But this may not make a big difference, because when one uses smaller Ω , then a smaller A would be able to generate the same bandgap, as we described above. Hence, the $\frac{A}{\Omega}$ can be kept relatively small even if Ω is small.

3 Spin Hall Conductivity

We have also calculated the spin Hall conductance based on the Kubo-formula

$$\sigma_{ab}^{s_i} = \frac{e^2}{\hbar} \sum_{n \neq m} \frac{dk}{(2\pi)^2} (f_n - f_m) \frac{\text{Im} \{ \langle m | j_a^i | n \rangle \langle n | v_b | m \rangle \}}{(\omega_m - \omega_n)^2} \quad (\text{S14})$$

Here $j_a^i = \frac{1}{2}(s^i v_a + v_a s^i)$ is the spin current operator. We focus on the spin current with spin- z polarization $\sigma_{ab}^{s^z}$. The layer-resolved spin Hall conductance of a slab system with 24 quintuple layers (QLs) is shown in Figure S3. One can see that the middle layers have spin Hall conductance around $0.36 \frac{\hbar}{2e} \frac{e^2}{h}$, which is very close to the value when the layer is put in the bulk system (dash horizontal line).

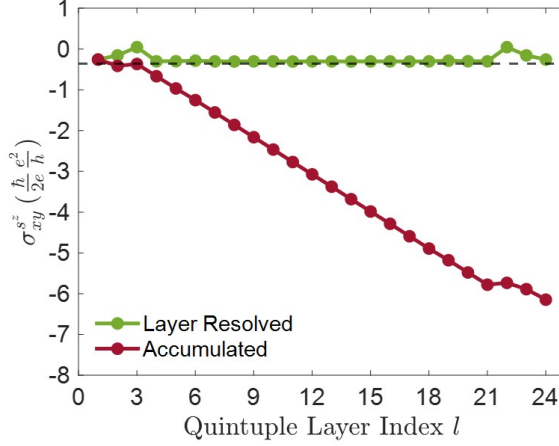


Figure S3: The spin Hall conductance of a Bi_2Si_3 slab system with 24 quintuple layers. The dashed horizontal line is the spin Hall conductance per layer when the layers are put in the bulk system.

In Figure S4 we plot the the spin and charge Hall conductance per layer of bulk Bi_2Si_3 . One can see that A field strength of $\frac{eA}{\hbar} = 0.05 \text{ \AA}^{-1}$ is not enough to trigger the phase transition to quantum anomalous Hall insulators in the bulk.

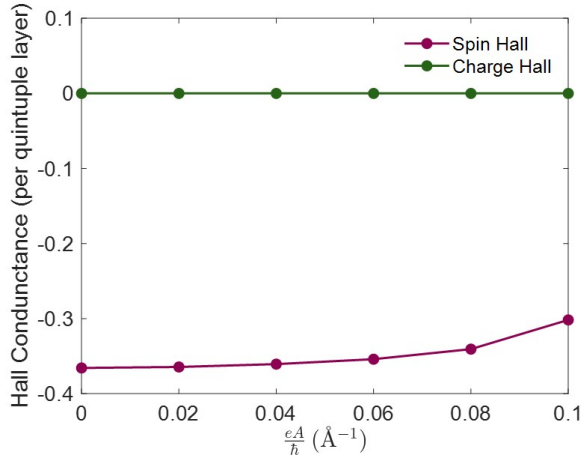


Figure S4: The Hall conductance of a quintuple layer in the bulk Bi_2Si_3 as a function of the strength of the circularly polarized light. A field strength of $\frac{eA}{\hbar} = 0.05 \text{ \AA}^{-1}$ is not enough to trigger the phase transition to quantum anomalous Hall insulators in the bulk, thus the charge Hall conductance is always zero. On the other hand, the spin Hall conductance is about $0.36 \frac{\hbar}{2e} \frac{e^2}{h}$, and slightly varies with the field strength.

References

- [1] Hohenberg, P. & Kohn, W. Inhomogeneous electron gas. *Physical review* **136**, B864 (1964).
- [2] Kohn, W. & Sham, L. J. Self-consistent equations including exchange and correlation effects. *Physical review* **140**, A1133 (1965).
- [3] Kresse, G. & Furthmüller, J. Efficiency of ab-initio total energy calculations for metals and semi-conductors using a plane-wave basis set. *Computational materials science* **6**, 15–50 (1996).
- [4] Kresse, G. & Furthmüller, J. Efficient iterative schemes for ab initio total-energy calculations using a plane-wave basis set. *Physical review B* **54**, 11169 (1996).
- [5] Perdew, J. P., Burke, K. & Ernzerhof, M. Generalized gradient approximation made simple. *Physical review letters* **77**, 3865 (1996).
- [6] Blöchl, P. E. Projector augmented-wave method. *Physical review B* **50**, 17953 (1994).
- [7] Mostofi, A. A. *et al.* An updated version of wannier90: A tool for obtaining maximally-localised wannier functions. *Computer Physics Communications* **185**, 2309–2310 (2014).
- [8] Shirley, J. H. Solution of the schrödinger equation with a hamiltonian periodic in time. *Physical Review* **138**, B979 (1965).
- [9] Sambe, H. Steady states and quasienergies of a quantum-mechanical system in an oscillating field. *Physical Review A* **7**, 2203 (1973).
- [10] Eckardt, A. Colloquium: Atomic quantum gases in periodically driven optical lattices. *Reviews of Modern Physics* **89**, 011004 (2017).
- [11] De Giovannini, U. & Hübener, H. Floquet analysis of excitations in materials. *Journal of Physics: Materials* **3**, 012001 (2019).